Effects of Leading-Edge Tubercles on the Generation of Lift by NACA 4412 Airfoil

Pranaav Makharia

This paper explores the tubercle effect on the generation of lift by airfoils by utilizing 3D printed versions of the NACA 4412, 0012, and 2412. Existing work often uses specialized or symmetric sections at more ideal conditions utilizing lab grade wind tunnels and load cells [1][2][3], but the results created by the tubercle effect on a cambered airfoil (the NACA 4412) that is commonly used at a lower flow velocity value remain more obscure [2][3]. To test the tubercle effect on the cambered airfoil, a custom open-circuit wind tunnel was constructed where multiple tests were run at different wind speeds to measure the lift generated by the airfoils at multiple angles of attack. Each test point was repeated twice for repeatability, where the fan speed and pressure differentials were measured using an Arduino UNO. The results at the highest fan speed available (Re of ~3.1×10^4 to ~3.7×10^4) showed that the tubercled NACA 4412 produced a higher mean C_L than the base variant, most visibly at angles of attack 10°-15°, where at 15° the tubercled wing had mean C_L of 0.96 while the base variant had mean C_L of 0.85 (a 13% difference). No stall was visible in the tested ranges, and thus the classic claim of delayed stall was not verified here.

I. Nomenclature

P	=	Pressure [Pa]
$P_{dynamic}$	=	Dynamic Pressure [Pa]
v_{flow}	=	Velocity of the Oncoming Air Flow [m/s]
ρ	=	Density of Air [kg/m^3]
Re	=	Reynolds Number
c	=	Chord Length [m or cm]
S	=	Planform area [m^2 or cm^2]
ν	=	Kinematic Viscosity [m^2/s]
m	=	Mass [g or kg]
L	=	Lift Generated [N]
g	=	Acceleration Due to Gravity [m/s^2]
D	=	Drag Generated [N]
α	=	Angle of Attack [°]

Δh = The Difference in Height Between the Leading and Trailing Edge [cm]

M = Mach Number

a = Speed of Sound in the Tunnel

γ = Specific Heat Ratio of Dry Air

R = Specific Gas Constant [J/(kg·K)]

T = The Absolute Temperature [K]

C_L = Coefficient of Lift

C_D = Coefficient of Drag

II. Introduction

The most iconic feature of an airplane is, undoubtedly, the pair of large and intricately designed wings by its sides. This pair of wings can vary in multiple different manners, namely, material, length, and camber, or, the asymmetrical curvature of a wing from its leading edge (front) to the trailing edge (back.) All these variables contribute to the main goal of the wing, or more technically named airfoil, which is to generate lift. Lift is the force that is generated by a difference in pressure above and below the airfoil that pushes the airplane upwards and the reason that airplanes can function in the first place. The generation of lift is also dependent on another key aspect: the angle of attack. The angle of attack is the angle at which the airfoil is positioned in comparison to its chord line (the horizontal) and the oncoming flow. Most commercial and popular airfoils often have a low stall margin, meaning the angle of attack where they generate high amounts of lift is very close to the angle of attack where the amount of lift generated vastly falls off. The stall margin is defined as the “buffer zone” between where an airfoil can generate high lift at one angle of attack before falling off at a higher angle of attack. It can be pictured as being positioned next to a large cliff in front of you, where having a low stall margin means that you only have a few steps you can take before you fall off (ie a small difference in the angle of attack), and having a high stall margin indicates that you may take many steps before you fall off (a larger difference in the angle of attack).

There is a field of study which aims to make airfoils more efficient in multiple regards, that field being Biomimetics. Biomimetic airfoils are standard airfoils that have been modified to replicate certain features of the world’s fauna in order to perform better in a multitude of things such as providing the ability to glide, reduce noise pollution, increasing stall margin, and more. Some existing concepts of the biomimetic airfoil utilize things such as owl wings and their ridged geometry to remove noise pollution, while others may utilize shark-like scales to create greater lift on an airfoil by creating drag-reducing riblets. Some even attempt to use the biomimetic airfoils in terms of car-based aerodynamics [4]. This paper itself focuses on increasing the lift generated at higher angles of attack. To increase the generation of lift for the

NACA 4412 airfoil (National Advisory Committee for Aeronautics) humpback whale pectoral flippers were utilized. Humpback whales have small (relative to the whale itself), rounded follicles on the leading edge of their pectoral flippers that are referred to as tubercles. The tubercles themselves serve to create counter-rotating streamwise vortices, and in doing so improves maneuverability for the humpback whale [1]-[3]. The question this paper aims to answer was whether leading edge tubercles would lead to the generation of increased lift, namely, at higher angles of attack, although Miklosovic et al. [1], [2] and Johari et al. [3] indicate that leading edge tubercles may produce reduced lift prior to stall.

In approaching this question, it was hypothesized that the tubercle version of the NACA 4412 will effectively increase the lift generated at higher angles of attack than that of the original NACA 4412. This paper describes the creation of a wind tunnel, methods of data gathering and comparison of multiple different airfoils, (the NACA 4412, NACA 0012, NACA 2412, and the biomimetic NACA 4412) for the purposes of answering the question of the effectiveness of this particular biomimetic design in improving the generation of lift.

III. Methodology

3.1 Wind Tunnel

The custom wind tunnel that was constructed is an open-circuit wind tunnel. It consists of a 3-speed fan with a plywood settling chamber, contraction, acrylic test chamber, and plywood diffuser. The tunnel's flow visualizer tube is multiple straws cut and glued together, placed at the front of the test chamber. The settling chamber has a 3D printed honeycomb structure inside it that serves to straighten the oncoming flow [7].



Figure 3.1.1: *The above image depicts the wind tunnel that was constructed, alongside the flow visualization method utilized, which was a small method of fog production.*

3.2 Data Gathering & Equipment

For the wind tunnel to actually be utilized, there are multiple different tools that were utilized to gauge and gather relevant data. To measure the velocity, differential pressure, and the Reynolds Number within the wind tunnel, the MPXV7002DP Differential Pressure sensor was utilized alongside an Arduino Uno to gather information. The differential pressure sensor was attached to two pitot probes (the static and total pitots). The static pitot probe consists of a straw with a sealed end and small ~1-2 mm holes placed in the top of the straw perpendicular to oncoming flow. The total pitot probe also simply consists of a bent straw, held in place with a bead of hot glue. Both of these pitot probes protrude from the test chamber, upstream of the

placement of the airfoil, and use silicon tubing to reach the differential pressure sensor, which is subsequently attached to the Arduino Uno, where the data outputs are recorded in the Arduino IDE. Prior to each trial and airfoil test, the sensor was zeroed with the wind tunnel off, i.e., resetting the initial conditions. Finally, a flow visualizer was also constructed from multiple pieces of straw with a sealed end that was placed in the test chamber, with fog fed through the top of the visualizer.

The pitot probe set up measures the total and static pressure as indicated by the respective probe names. Thus the dynamic pressure, $P_{dynamic}$, as follows:

$$P_{dynamic} = \Delta P = P_{total} - P_{static} \quad \text{Eq 1}$$

The difference in pressure is calculated by the Arduino Uno and is output directly to the Arduino IDE 5 times per second (as are the velocity of the oncoming flow and the Reynolds Number). $P_{dynamic}$ was then utilized to find the velocity of the oncoming flow, v_{flow} in the following set up in the Arduino by rearranging Bernoulli's Equation:

$$v_{flow} = \sqrt{\frac{2\Delta P}{\rho}} \quad \text{Eq 2}$$

Similar to the dynamic pressure, the velocity of the oncoming flow was output 5 times per second onto the Arduino IDE. Knowing velocity provides sufficient to find the Reynolds Number within the tunnel, where the arduino utilizes the following equation to calculate the value and output it onto the IDE:

$$Re = \frac{v_{flow} c}{\nu} \quad \text{Eq 3}$$

The Reynolds Number was also output onto the Arduino IDE 5 times per second, meaning the final results utilize the averaged version, as they do for velocity, and for the dynamic pressure.

For the purpose of finding the lift generated by the airfoil, a simple kitchen scale was used and stuck the airfoil to the scale. After doing so, the kitchen scale was turned on and tared prior to running a test (for the purpose of the airfoil and scale weighing 0 grams.) Afterwards, the "negative mass" reading on the scale was recorded. This allows us to find the change in mass as follows (taking into account unit conversions):

$$\Delta m = |m_{negative}|/1000 \quad \text{Eq 4}$$

From this point, with the change in mass being available, we can find the lift generated by the airfoil through the equation

$$L = \Delta m * g \quad \text{Eq 5}$$

From this point, the coefficient of lift may be found by:

$$C_L = \frac{2L}{\rho v_{flow}^2 S} \quad \text{Eq 6}$$

Finally utilize thermometers to measure the temperature in the wind tunnel at the beginning of the tunnel (by the fan), and at the test chamber, downstream of the airfoil. The result will allow us to find the temperature differential, which is the change in temperature from the start of the tunnel to downstream of the airfoil, which will be used later in discussing the results of the research.

3.3 Airfoils

There were two primary airfoils that were utilized, those being the basic NACA 4412 [6] and the Tubercle version of the NACA 4412. The base version of the NACA 4412 was a smooth and straight leading edge, while the tubercle version possessed a sinusoidal leading edge that mimicked the humpback whale's pectoral fin. Both the base and tubercle version of the NACA 4412 possessed a chord length of 10.1 centimeters and span of 10.1 centimeters. The amplitude of the tubercled version's leading edge is approximately 5.05 mm, where 4 tubercles are present [2]. Note that for the S value of the tubercled wing, the mean chord used was 0.101m (the leading edge amplitude was $\pm$ 5% of the chord, and there were four tubercles across the span). Both models were also 3D printed and sliced in Creality Cloud and produced using the SparkiX7 creality printer.

There is also the presence of 2 additional NACA airfoils, those being the NACA 0012 and the NACA 2412 [6], which were not altered for biomimetic purposes but rather kept to verify results of the wind tunnel and served as control variables to ensure that data is consistent with existing findings.

All models printed utilized the same Creality Cloud software, where the layer height for each model was 0.2 mm. The models were printed using PLA filament (cornstarch/sugarcane base), and printed in a vertical orientation for ease and speed of printing (where the flat faces of the airfoil are vertical). In doing so, it is important to note the possibility of slightly deforming the side edges of the airfoils, but this will not hamper results as the relative comparisons remain unhindered. Furthermore the airfoils underwent no sanding upon print, meaning they lack additional smoothness that may be typical of commercial airfoils.

All 4 of the models were tested at multiple different angles of attack, the base and tubercled NACA 4412 being tested at α values (angle of attack) 0º, 5º, 7.5º, 10º, 12º, 15º while the 0012 and 2412 were tested at only 0º and 5º. The set up for the sting and angle of attacks were a short wooden dowel that was hot glued to the kitchen scale, and a small popsicle stick platform that was placed on top of the dowel. The wooden platform was then offset by the appropriate angles of attack from the horizontal, or the direction of the oncoming flow, found by the following (in centimeters):

$$\Delta h = 10.1 sin(\alpha) \quad \text{Eq 7}$$

3.4 Procedure

For each respective airfoil, the following process was applied to gather the desired data, where angles of attack 0° and 5° were used for all airfoils, and 7.5°, 10°, 12°, and 15° were only utilized when testing both of the NACA 4412 variants. The following procedure was repeated twice for all 3 available fan speeds for each airfoil at every angle of attack:

1. Place the model on the sting, and verify the angle of attack, α, aligns with the value of Δh mentioned in the airfoil subsection of methodology.
2. Ensure the airfoil and kitchen scale are in the test chamber, relatively placed in the center horizontally, and tare the scale so that the initial mass is recorded as 0g. Note that taring the scale does remove the static weight of the sting and the airfoil, but does not account for aerodynamic force on the dowel and tilted platform,
3. Zero the pressure sensor through the Arduino IDE platform when the fan is not running.
4. Set the fan to the desired speed, and record the negative mass reading on the kitchen scale after ~20-30 seconds of the tunnel running, while also recording the difference in temperature from thermometer readings at the beginning of the tunnel and downstream the airfoil.
5. Record the values of $P_{dynamic}$, v_{flow}, and Re provided by the Arduino and differential pressure sensor at times past 20 seconds of run time (utilize a few instances of data, such as 5-10 outputs.)
6. Repeat the process once more at the same fan speed to identify any inconsistent data.

7. **Flow Visualization Step**: Flow visualization in the tunnel was difficult, as the fan speed was rather quick for any fog/smoke to appear on multiple runs. The process was simply to place the airfoil and turn on the fan at the lowest speed while feeding fog through it, this step was only properly visible on a few trials.

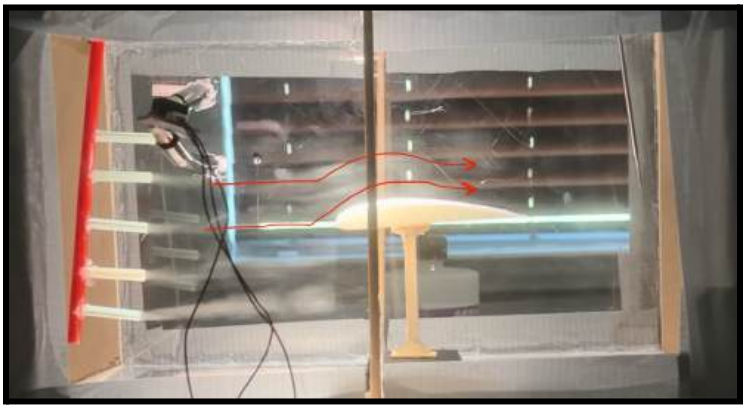


Figure 3.4.1: *The picture above is one of the few successful flow visualization runs, which depicts the fog creating a wake around the airfoil as indicated by the guidance arrows drawn on the image.*

IV. Results

Throughout the following, the 3rd fan speed (the fastest one) is the one plotted and considered in the figures. The differential pressure, velocity of the flow, and Reynolds number are all averaged values across two trials of the data set output by the Arduino UNO. Furthermore, the following use the planform area of the chord, S, as S = 0.101^2 meters, and the density of air is 1.225 kg/m^3.

4.1 Primary Results

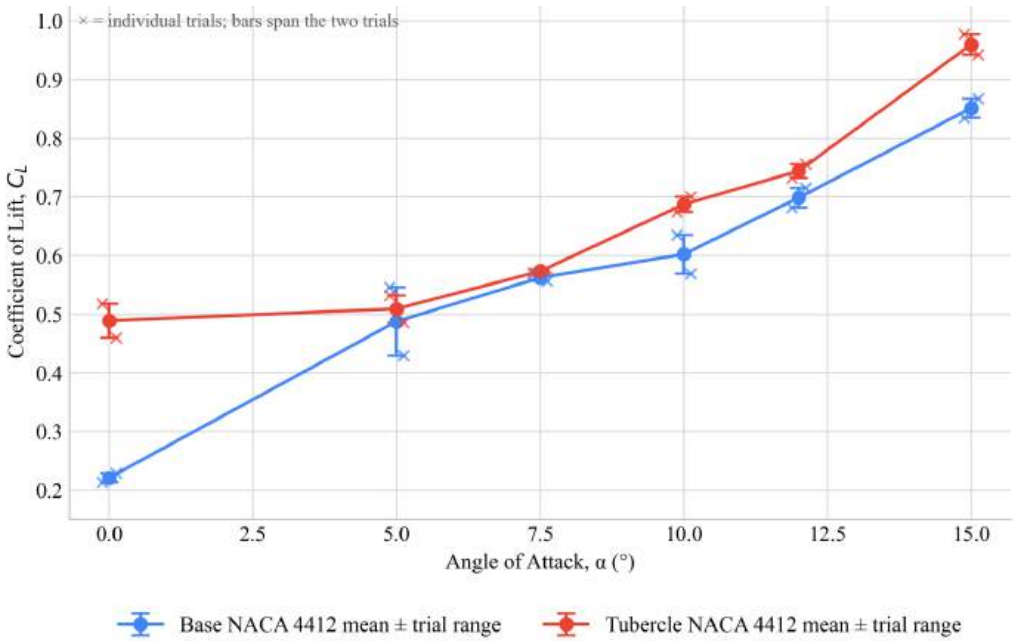


Figure 4.1.1*: This figure displays the graph of the Angle of Attack vs. The Coefficient of Lift, depicting the trends for both variants of the NACA 4412 tested, the two trials performed are averaged to yield the depicted data. The crosses are the individual trials that took place, and the error bar extends between both trials. The lines represent a mean value, not a fitted model.*

Both the base variant and tubercle variant of the NACA 4412 have a greater coefficient of lift (C_L) with an increase in the angle of attack (α), where the tubercled variant has a greater coefficient of lift at every point but not being equally as convincing at every point. At an angle of attack of 5° and 7.5°, the two points nearly overlap (with differences of only 4% and 2%). The difference in C_L values is most evident at α values 10°, 12°, and 15° (~ +14%, +6%, and +13% greater at those points respectively). The large gap at angle of attack 0° is reported but is treated as unreliable.

4.2 Data Quality and Variable Relations

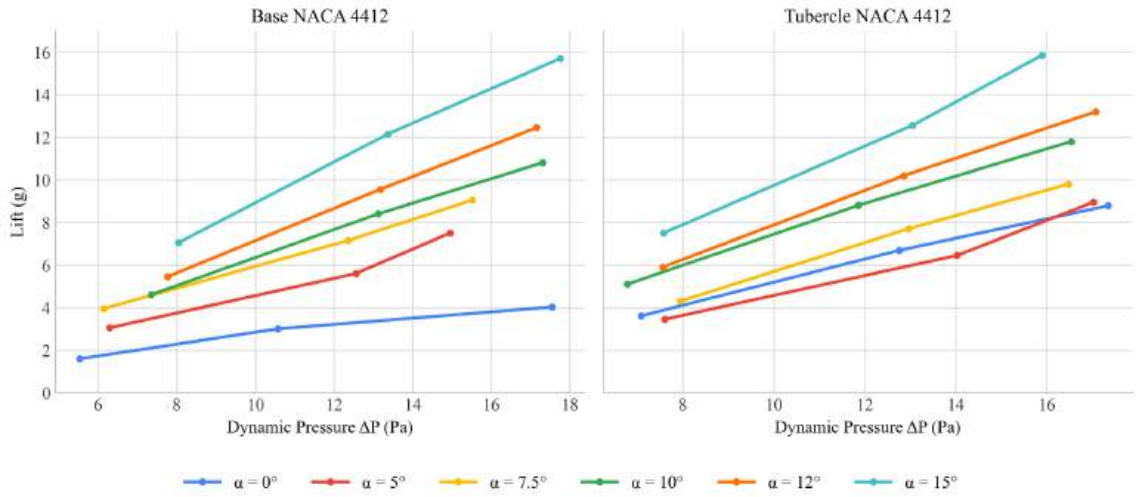


Figure 4.2.1*: This figure plots the change in pressure (the dynamic pressure) against the generated lift for the respective NACA 4412 Airfoils at different angles of attack.*

The data in **Figure 4.2.1** shows a nearly linear trend between the lift, which is measured in grams and not Newtons in this case. This indicates an internal consistency across trials. where the coefficient of determination is ~0.85-0.995 as indicated by the plotting software, meaning the variation in data is explained for the most part by the above model.

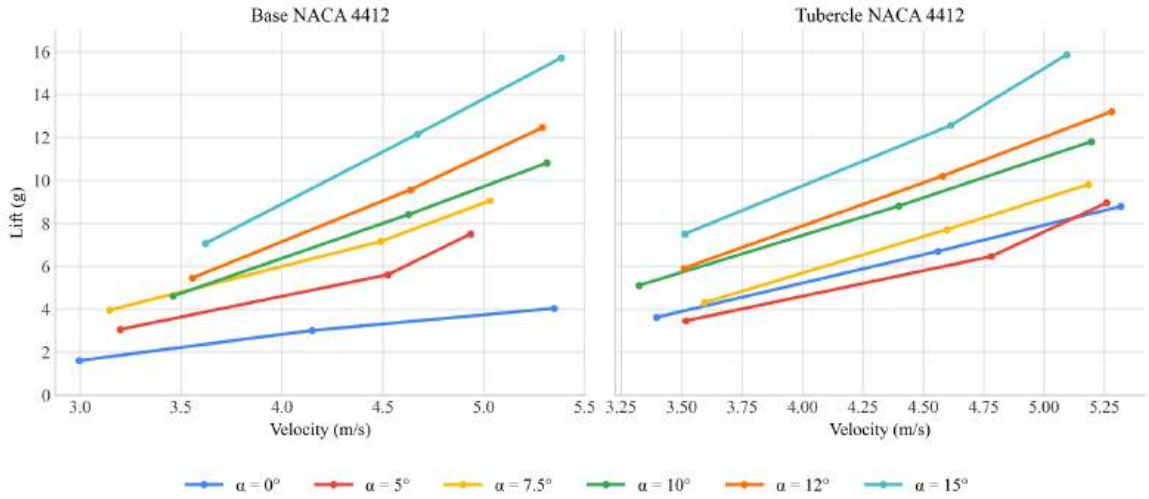


Figure 4.2.2: *The figure depicts the velocity against the lift (measured in grams) across different angles of attack.*

This figure, similar to 4.2.1, depicts a slight upwards curve, as $L \propto V^2$. The upwards curve is slight due there only being 3 available speeds, where the range of velocity is relatively narrow (~3-5.5 m/s), thus providing a less obvious visual relationship in the graph.

4.3 Nondimensional Data vs Flow Conditions

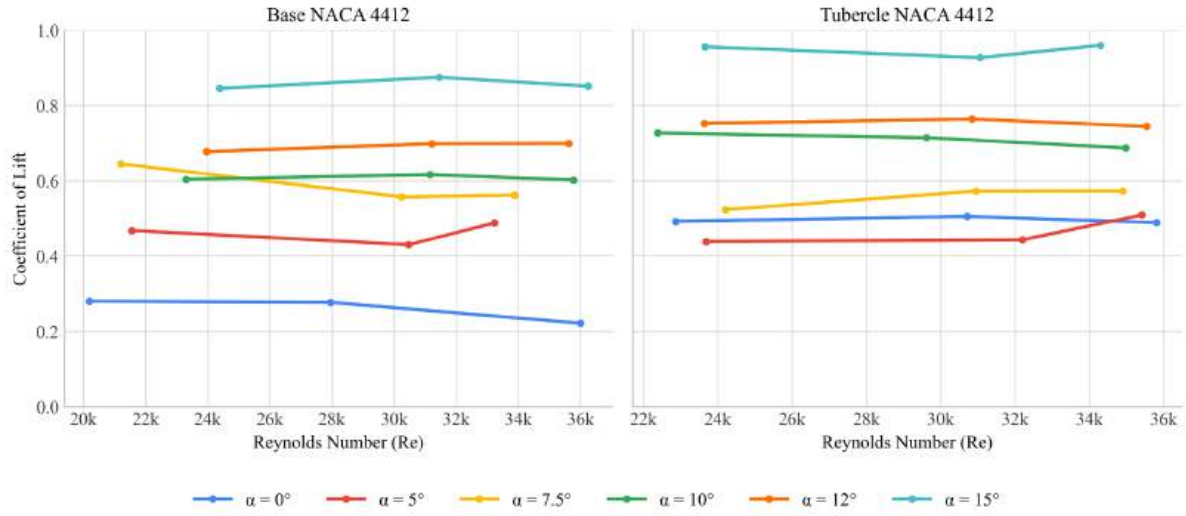


Figure 4.3.1: *Above are the graphs for the Reynolds Number versus the coefficient of lift for both the tubercled and base NACA 4412 across different values of* α.

The graphs in **Figure 4.3.1** provide a visual to display that the coefficient of lift is consistent and relatively constant across different Reynolds Numbers. Doing so supports the idea that regardless of speed, the coefficient of lift is consistent, even across only 3 tested speeds.

4.4 Verification of Data - 0012 & 2412 vs Airfoil Tools Data

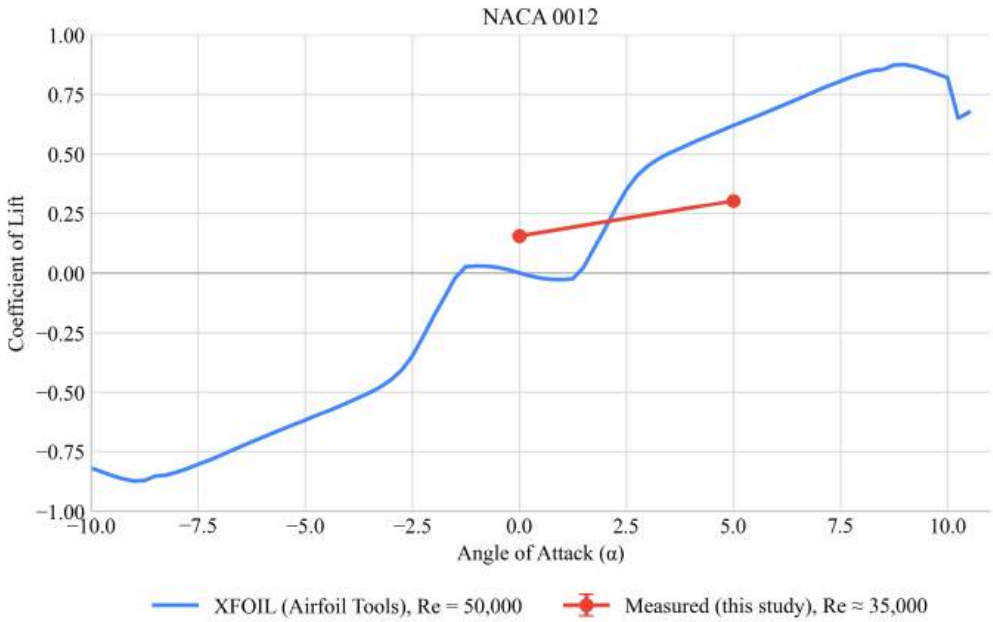


Figure 4.4.1*: The figure above is a compilation of data from Airfoil Tools [9][11] and the test data in this study for the NACA 0012 that plots the Angle of Attack against the Coefficient of Lift.*

The above figure serves to verify the trends in data for the NACA 0012 airfoil. Because only two angles of attack were tested for the study, the line is lacking data points and looks far more linear than the actual data.

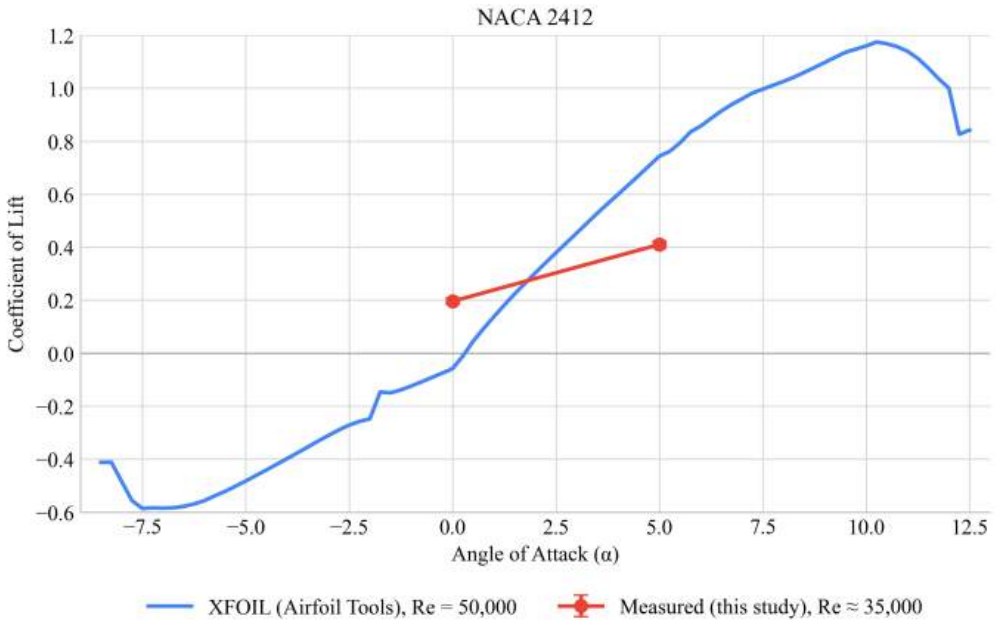


Figure 4.4.2: *This figure plots the angle of attack against the coefficient of lift for the NACA 2412 for this study against that of the data in Airfoil Tools [10][11].*

The graph here serves to verify the trends of the airfoils similar to the previous figure in this section. Once more, there is a lack of angles tested in this study, so the data looks more linear than it would be in reality.

V. Discussion of Results

5.1 Research Question

Throughout the study, the working hypothesis was that the tubercled version of the NACA 4412 will provide increased lift at higher values of α, a notion that was supported throughout the data. The value of $C_{L_{tubercle}} > C_{L_{base}}$ for all values of α from values of 0-15°, although there was near overlap at angles of attack 5° and 7.5°, making the later data points more convincing. When tested at the highest available speed, while also increasing with the angle of attack. At 15°, the highest angle of attack value tested, the coefficient of lift for the tubercled NACA 4412 versus the base version was ~0.96 vs ~0.86 respectively. The higher pre-stall C_L measured in this case, especially in consideration to lower angle of attack values, challenge the pre-stall trend depicted in some existing works [1][2][3]. Stall was not observed during these trials, and thus classic claims regarding stall and the tubercle effect cannot be verified here.

5.2 Flow Regime

Throughout all the trials, the velocity of the oncoming flow ranged from 3-5.5 m/s, meaning that the Mach Number (M) ranged from ~0.009 to ~0.016, indicating that the flow was incompressible and thus that a fixed air density was a reasonable assumption. To find the Mach number, the following equation was used:

$$M = \frac{v_{flow}}{a},\ a = \sqrt{\gamma \cdot R \cdot T} \qquad \text{Eq 8}$$

The temperature was recorded for each run, where the difference in temperature at the beginning of the tunnel and at the end of the tunnel was recorded. The difference in temperature was small throughout each trial, typically yielding a temperature differential of 0.2° Fahrenheit. This indicates that the temperature difference was not a major factor in the trends depicted in the results.

5.3 Tubercle Effect

The Tubercle Effect refers to the creation of counter-rotating streamwise vortices by the tubercle, which energizes the boundary layer, and allows the wing to generate greater lift at higher angles of attack due to a delayed separation of the laminar flow. The reason this effect is believed to be significant is because it performs the same job as conventional vortex generators but does so without increasing the drag penalty to the same extent [1][2][3]. Note that stall margin isn't referenced in this paper, as stall was unobserved, so this aspect of the Tubercle Effect will not be commented on here.

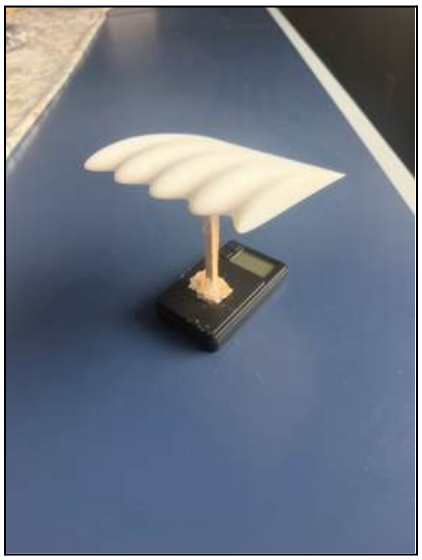


Figure 5.3.1*: This image above is a picture of the tubercled NACA 4412 that was utilized throughout the study, where the tubercle is visible on the leading edge of the airfoil.*

With this information, we may refer back to **Figure 4.1.1**, which depicts α vs C_L of the two variants of the NACA 4412. The data is consistent with the tubercle effect, as at higher angles of attack, the gap between the coefficient of lift for the tubercled 4412 and the base variant is

growing, although at an unsteady rate, as at 5°-7.5°, the difference in C_L is near 0, and the gap is widening between 10°-15°.

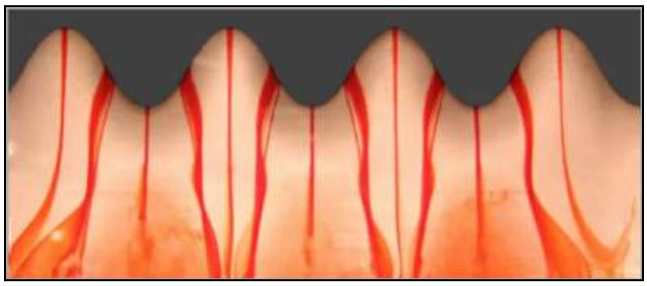


Figure 5.3.2: *The above image is taken from an existing paper by Krishnamurthy [5] that depicts the oncoming flow on a tubercled airfoil, where the flow is represented by the red dye that hugs the tubercles, allowing for the greater production of lift due to delayed separation of flow.*

Note that the odd initial gap between the coefficient of lift for the two variants at 0° is not necessarily a result solely of generation of extra lift by the tubercle effect, but may be influenced by the mounting geometry of the airfoil sting.

Nonetheless, the largest difference between the two variants is the presence of tubercles, meaning that the pattern is consistent with the proposed tubercle method, although this alone does not provide sole proof, as flow separation was not observed directly, and the mounting angle may have been inconsistent. Rather than prove the tubercle effect, we can simply see trends that are consistent with the notion that lift generated would be increased for the biomimetic NACA 4412.

5.4 Comparison of Test Data and Existing Polars of NACA 0012 and 2412

It is important to note this data verification section serves to display that the trends match what was expected, but the C_L values differ from that of the 2D XFOIL for known reasons [11]. These reasons come from the fact that 2D XFOIL is simulated across an infinite span, whereas in this study, we simply use $S = 0.101^2 = 0.010201$ m^2, causing air to spill around the wings and leading to a smaller growth in the value of C_L than a wing with infinite span. The standard finite-wing approximation predicts the slope will be 0.026 per degree for a square wing (even dimensions) and the slope measured for the tunnel is 0.030 and 0.043 for the NACA 0012 and the 2412, displaying relative trend agreement with the predictions. The steeper slope for the 2412 is only partly explained by the finite-wing approximation, as camber and measurement scatter affect the variables as well. Another point to consider is that the polars given by *Airfoil Tools* utilize, at the lowest, a Re value of 50,000 [9][10], while the highest Re value in this study is only 35,000, yielding different conditions for the airfoils. Furthermore, lift was measured using a kitchen scale, not a load cell, leaving room for error for issues with taring and consistency among measurements. Finally, the last known reason is possible bias with the mounting of the airfoil upon the sting, where the initial values of α could have been slightly greater than 0, thus leading to a higher absolute value of C_L at $\alpha = 0^o$. This means that even for the NACA 4412 Base and Tubercle variants, the comparison is still usable

since both utilize the same relative conditions, even if the absolute value may be biased, as the internal conditions themselves also prove relatively stable as is visible by **Figure 4.2.1** and **Figure 4.2.2**, which display the adherence of the relationship between lift and the pressure and velocity respectively. *Airfoil Tools* also has 2D XFOIL polars for the basic NACA 4412, and this polar was used for relative reference, but not as a quantitative control because of the aforementioned reasons regarding the NACA 0012 and 2412 [8]. This explanation regarding angle offset would also explain why the NACA 0012, which shouldn't generate any lift at an angle of attack of 0°, where the approximate true angle of attack could be found as $\alpha_{true} \approx \frac{0.154}{0.030} \approx 5°$ (by dividing the C_L by the measured slope of 0.030). The statement regarding the angle offset likely is present for all the trials. Thus, absolute values of C_L based on values of alpha should be interpreted with a level of caution, especially at 0°, although relative trends still hold.

5.5 Uncertainties

Although the lift was able to be effectively tested, the effects of Tubercles on stall margins was not resolved, as no visible stall effects were present at the angles of attack tested. Thus no claims about the stall margin will be made throughout this paper, despite existing claims that the stall margin is delayed by the tubercle effect [1][2][3].

Throughout testing, it is also possible that there was force contamination, and that drag could've affected the kitchen scale measurements which were taken, for example, the lift could have had a lower reading as a result of the drag applying a downward force (reducing the negative mass reading on the kitchen scale). Furthermore, the wind tunnel was open-circuit, meaning there is a possibility of outside conditions affecting internal results, due to such things as taking in ambient, surrounding air, exposing the airfoil to possibly different conditions than the more isolated closed-circuit wind tunnel. Furthermore, the honeycombs and airfoils themselves were 3D printed, meaning they don't have the precision that industrial grade airfoils would have, and can be open to minor discrepancies amongst pieces, or misaligned filament placing.

The Pitot set up was also a DIY set up composed of straws, meaning that readings could be slightly biased or inaccurate due to the nature of DIY work. It is important to note that dynamic pressures were measured to be about 14-18 Pa only (speed 3). With the 10-bit Arduino UNO ADC and the MPXV7002DP $\pm$ 2 kPa Pressure sensor, pressure noise can be a large contributor to the value of C_L. This is visible by substituting Equation 2 into Equation 6, which yields that $C_L = \frac{L}{\Delta P \cdot S}$, meaning the noisy pressure directly could have affected the value of the coefficient of lift. It is also worth noting that the aspect ratio of the airfoils was 1, and that they sat relatively close to the tunnel floor and the walls, meaning interactions between these can possibly have affected lift. The tunnel uniformity, turbulence intensity and steadiness were not measured, and in future work a handheld anemometer would help verify and would strengthen confidence.

A glaring point to consider is the odd lift reading at the 0° angle of attack for the tubercled NACA 4412, and caution should be taken when drawing conclusions from this point in particular. In light of the change in C_L values for the tubercled NACA 4412 from angles of

attack 0° to 5° (0.489 to 0.509) compared to that of the basic NACA 4412 (0.221 to 0.487), the claim that both foils experienced identical relative conditions holds less weight at $\alpha = 0$ specifically. It should also be noted that the ideal practice in finding absolute readings would take sting and scale only runs in the wind tunnel, and utilize these readings to be subtracted from the airfoil, sting and platform readings, but was not done here and is thus a limitation of the study.

VI. Conclusion

This study compared the basic NACA 4412 and the tubercled version of the NACA 4412 in a custom made open-circuit wind tunnel. The measurements of this tunnel were taken through various methods, including a pitot-Arduino set up. Throughout the testing, it was evident that the coefficient of lift generated by the tubercled version was greater for every angle of attack than that generated by the base version, although the difference in the value of C_L varied with increasing angles of attack, and measured values presented concern at $\alpha = 0°$. These results support the initial hypothesis that the tubercled model will produce a higher coefficient of lift than the basic version even in the low Reynolds number set up present for this study, and stall was not reached throughout the study and was thus not measured nor commented on.

Higher values of C_L for the tubercle variant of the NACA 4412, most notably at 10°-15°, suggest the potential application of the design in limited lift conditions. This difference, if confirmed with more accurate angle calibration, could possibly indicate increased generation of lift at lower airspeeds and lower angles of attack, or being able to support a higher load at the same speed or angle of attack.These points may be relevant during short duration phases of an aircraft, such as climbing, takeoff, etc (notably for small aircraft). These are only possible applications however, as they were not explicitly studied and drag, lift-to-drag ratio, flight performance, and stall behavior were not taken into account during this study, and previously mentioned points of concern may limit the interpretation of low α results.

Although the NACA 0012 and 2412 were not identical to the polars, the trends were accurate and were deduced to known reasons such as airfoil span, differing Re conditions, DIY methods of lift measurement, and possible inaccuracy in values of the angle of attack of the sting. These limits themselves do not necessarily impede the comparison made between the base and tubercle version, as it is a relative comparison which utilized the same facility and procedures

In the future, more values of α for testing to effectively gauge stall margin differences generated by the tubercle effect, and to improve methods of data gathering by possibly utilizing a load cell to also identify drag. Furthermore, more varied wind speeds will be tested for the purpose of testing at different values of Re to utilize data that is able to be more accurately compared to the existing data online. A more fleshed out flow visualization system will be incorporated to more accurately retain a visual, and to match existing polars. Future revisions will also include sting-only runs in the wind tunnel, and a more reliable method of verifying 0° angles of attack.

Sources

References and Existing Research Utilized

[1] D. S. Miklosovic, M. M. Murray, L. E. Howle, and F. E. Fish, “Leading-edge tubercles delay stall on humpback whale (Megaptera novaeangliae) flippers,” Phys. Fluids, vol. 16, no. 5, pp. L39–L42, May 2004, doi: 10.1063/1.1688341.

[2] D. S. Miklosovic, M. M. Murray, and L. E. Howle, “Experimental evaluation of sinusoidal leading edges,” J. Aircr., vol. 44, no. 4, pp. 1404–1408, Jul. 2007, doi: 10.2514/1.30303.

[3] H. Johari, C. Henoch, D. Custodio, and A. Levshin, “Effects of leading-edge protuberances on airfoil performance,” AIAA J., vol. 45, no. 11, pp. 2634–2642, Nov. 2007, doi: 10.2514/1.28497.

[4] H. Ghaffar, H. Yusoff, D. Ibrahim, S. Budin, and M. R. A. Razak, “A simulation study of tubercles effect of aerodynamics performance on car rear spoiler,” J. Phys.: Conf. Ser., vol. 1349, no. 1, Art. no. 012034, 2019, doi: 10.1088/1742-6596/1349/1/012034. [Online]. Available: https://ui.adsabs.harvard.edu/abs/2019JPhCS1349a2034G/abstract

[5] R. Krishnamurthy, “A whale of an idea in wing design,” GridPro Blog, Jul. 8, 2019. [Online]. Available: https://blog.gridpro.com/a-whale-of-an-idea-in-wing-design/

[6] Designer, “NACA Airfoils (10 Models available including NACA-2412!),” Printables, Oct. 19, 2024. [Online]. Available: https://www.printables.com/model/1044758-naca-airfoils-10-models-available-including-naca-2

[7] Navadeep C K, “Honey Comb IA,” GrabCAD. [Online]. Available: https://grabcad.com/library/honey-comb-ia-1

[8] Airfoil Tools, “NACA 4412 (naca4412-il) XFOIL polar at Re = 50,000, Ncrit = 9,” Airfoil Tools. [Online]. Available: http://airfoiltools.com/polar/details?polar=xf-naca4412-il-50000

[9] Airfoil Tools, “NACA 0012 (n0012-il) XFOIL polar at Re = 50,000, Ncrit = 9,” Airfoil Tools. [Online]. Available: http://airfoiltools.com/polar/details?polar=xf-n0012-il-50000

[10] Airfoil Tools, “NACA 2412 (naca2412-il) XFOIL polar at Re = 50,000, Ncrit = 9,” Airfoil Tools. [Online]. Available: http://airfoiltools.com/polar/details?polar=xf-naca2412-il-50000

[11] M. Drela, “XFOIL: An analysis and design system for low Reynolds number airfoils,” in Low Reynolds Number Aerodynamics (Lecture Notes in Engineering, vol. 54), T. J. Mueller, Ed. Berlin, Germany: Springer, 1989, pp. 1–12.

Appendices

Appendix A - Tunnel and Model Geometry

The wind tunnel was open to room air that entered through the inlet/fan section, traveled through a settling chamber (~45.5 x 45.5 cm) which contained a honeycomb flow straightener

(matching dimensions), followed by a contraction with a cross-section of ~21.5 x 21.5 cm followed by a rectangular acrylic test section (~21.5 x 21.5 cm) The airflow followed and exited through the diffuser with a cross section of ~27.2 x 28.5 cm, while being driven forward by Lasko 20" 3-Speed Weather-Resistant Motor Box Fan B20200. The honeycombs were 3D printed in four separate parts and later stuck together, while being ~64 mm (63.5 mm) thick, where each honeycomb cell was 12 mm (top to bottom of the cell), and a wall thickness of ~1.6mm [7]. The length of the sections of the wind tunnel are as follows; settling chamber, 45.5 cm; contraction, ~30.5 cm; test chamber, 33 cm; diffuser, ~56 cm (total 165 cm in length.)

The mean chord and span of the airfoils were 0.101 m, meaning the area, S, is simply $.101^2$ m^2 throughout all calculations performed [6]. The tubercled version of the NACA 4412 has a peak-to-peak variation of 0.0101 m, or 10% of the chord, with a total of 4 tubercles across the span.

Appendix B - Sample Calculations

Constants that were used throughout the paper include:

- $\rho = 1.225\ kg/m^3$ for air density
- $\nu = 1.5 \times 10^{-5}\ m^2/s$ for kinematic viscosity
- $g = 9.81\ m/s^2$ for the acceleration due to gravity
- $a = 343\ m/s$ is the speed of sound in air at room temperature.

Note that the temperature in the wind tunnel ranged from 299-303 K, meaning a~ 346-349 m/s, but the change is negligible for the purposes of calculations, as the result of incompressibility is the same. Also note that the given density of air and kinematic viscosity are more standard for ~15° C. When solving for C_L, this difference does not affect results, but the reported velocity and Reynolds number would shift by a small percentage (~2.2% higher and 2.9% lower, respectively).

The following sample calculation will be performed for the Base NACA 4412, at an angle of attack of 10°, fan speed 3 (fastest) and the first trial. The averaged arduino values are as follows:

$P_{dyanmic}$=16.667 Pa v_{flow}=5.215 m/s Re=35115

1. Velocity from the change in pressure

$$v_{flow} = \sqrt{\frac{2\Delta p}{\rho}} = \sqrt{\frac{2\times 16.667}{1.225}} = 5.215\ m/s$$

2. Reynolds Number

$$Re = \frac{v_{flow} c}{\nu} = \frac{5.215\times 0.101}{1.5\times 10^{-5}} = 3.51 \times 10^4$$

3. Mach Number

$M = \frac{v_{flow}}{a} = \frac{5.215}{343} = 0.015$ (far less than 0.3, thus is incompressible.)

4. Lift From Kitchen Scale

$L = |\Delta m|g = (11.0/1000) \cdot 9.81 = 0.10791\ N$

5. Coefficient of Lift

$C_L = \frac{2L}{\rho v_{flow}^2 S} = \frac{2\times0.10791}{1.225\times(5.215)^2\times0.010201} = 0.635$

Appendix C - Organized Trial Data (Speed 3)

Table C1: Base and Tubercle NACA 4412 at the third fan speed. The temperature is in °F.

α (°)	Airfoil	Trial	Avg ΔP (Pa)	Avg V∞V∞ (m/s)	Avg Re	|Δm| (g)	C_L	Temp start→end
0	Base	1	17.601	5.358	36082	3.9	0.213	83.0→83.3
0	Base	2	17.497	5.337	35930	4.153	0.229	81.5→81.9
0	Tubercle	1	16.6	5.203	35034	8.923	0.518	82.8→82.8
0	Tubercle	2	18.102	5.433	36580	8.64	0.46	83.1→83.5
5	Base	1	13.748	4.735	31883	7.8	0.546	79.3→79.5
5	Base	2	16.163	5.135	34572	7.2	0.429	81.9→82.2
5	Tubercle	1	16.415	5.155	34709	9	0.532	79.5→79.9
5	Tubercle	2	17.644	5.363	36113	8.9	0.486	80.7→81.1
7.5	Base	1	15.269	4.99	33600	9	0.568	79.3→79.5
7.5	Base	2	15.78	5.072	34148	9.1	0.556	82.4→82.7
7.5	Tubercle	1	16.378	5.169	34803	9.7	0.57	78.1→78.4
7.5	Tubercle	2	16.583	5.197	34991	9.9	0.576	79.2→79.7

10	Base	1	16.667	5.215	35115	11	0.635	85.3→85.5
10	Base	2	17.952	5.411	36431	10.6	0.569	85.5→85.6
10	Tubercle	1	17	5.267	35462	11.9	0.674	81.7→81.9
10	Tubercle	2	16.082	5.122	34491	11.7	0.7	82.2→82.4
12	Base	1	17.63	5.363	36112	12.5	0.682	79.9→80.1
12	Base	2	16.684	5.217	35129	12.4	0.715	80.1→80.2
12	Tubercle	1	17.618	5.361	36096	13.4	0.732	80.2→80.4
12	Tubercle	2	16.557	5.197	34990	13	0.756	80.4→80.6
15	Base	1	18.319	5.467	36812	15.9	0.835	80.4→80.6
15	Base	2	17.201	5.299	35676	15.5	0.867	80.6→80.8
15	Tubercle	1	15.656	5.055	34032	15.9	0.977	80.6→80.8
15	Tubercle	2	16.147	5.133	34559	15.8	0.942	81.0→81.2

Table C2: Fan speed 3 trial-averaged values of C_L.

α (°)	Base Version C_L	Tubercle Version C_L	Avg v_{flow} Base Version/Tubercle Version [m/s]
0	0.221	0.489	5.35 / 5.32
5	0.487	0.509	4.93 / 5.26
7.5	0.561	0.573	5.03 / 5.18
10	0.602	0.687	5.31 / 5.19
12	0.699	0.744	5.29 / 5.28
15	0.851	0.959	5.38 / 5.09

Table C3: Control airfoils' C_L at fan speed 3.

α (°)	NACA 0012 C_L	NACA 2412 C_L
0	0.154	0.195
5	0.302	0.41